CPP

Contributions to Plasma Physics

www.cpp-journal.org

WILEY-VCH

REPRINT

Contrib. Plasma Phys. **49**, No. 4-5, 199 – 214 (2009) / **DOI** 10.1002/ctpp.200910023

Modelling of Voids in Complex Radio Frequency Plasmas

W.J. Goedheer[*1], **V. Land**[2], and **J. Venema**[1]

[1] FOM Institute for Plasma Physics Rijnhuizen, Nieuwegein, The Netherlands, www.rijnh.nl
[2] Center for Astrophysics, Space Physics and Engineering Research, Baylor University, Waco, Texas 76798, USA

Received 14 December 2008, accepted 26 March 2009
Published online 2 June 2009

Key words Complex plasma, RF discharges, hydrodynamic modelling, kinetic modelling, dusty plasma.
PACS 52.65.-y, 52.25.Vy,52.27.Lw

In this paper hydrodynamic and kinetic approaches to model low pressure capacitively coupled complex radio-frequency discharges are discussed and applied to discharges under microgravity. Experiments in the PKE-Nefedov reactor on board the International Space Station, as well as discharges in which gravity is compensated by means of thermophoresis are simulated with a 2-D cylindrically symmetric hydrodynamic model. Kinetic effects are studied with a 1-D Particle-In-Cell plus Monte Carlo model in which capture and scattering by dust grains is included. Simulations with this model address non-local effects and modulated discharges.

1 Introduction

Apart from electrons and ions, complex plasmas contain dust grains with a size ranging from a few nanometers to several microns. Usually, these grains obtain a large negative charge of approximately 2-3 electrons per nm radius. When their number density is high enough they have a significant influence on the plasma properties. On the other hand, the properties of the grains like the charge and density distribution depend on the plasma parameters. The result is a strongly coupled system, in which the grains can become so closely packed that their Debye sheaths start to overlap, eventually leading to incompressibility of the dust cloud and crystal formation. Complex plasmas thus form a colloidal system that is well suited to study kinetic aspects of solid state physics and fluid dynamics, on a scale visible to the eye. Typical topics are wave propagation, Mach cones, viscosity, turbulence, phase transitions, rheology, lane formation, etc. [1–8]. Obviously, for studies in three dimensions the formation of a sufficiently large homogeneous spatial distribution of grains is of great importance. On earth, however, for large grains gravity is the dominant force, and when this force is counteracted by the electric field above the lower electrode of a discharge, only thin, essentially two-dimensional structures can be made. The study of three-dimensional distributions requires the compensation or elimination of gravity. This can be done by applying a temperature gradient that creates a thermophoretic force [9–11], or by performing experiments under micro-gravity conditions during parabolic flights or on board space stations like the MIR or ISS.

The study of complex plasmas under micro-gravity [12, 13] revealed that for micron sized particles the dust distribution contained a dust free center, a so-called void. Initially, thermophoresis and the ion drag force were believed to be responsible for its generation, but the thermophoretic force was too small to play a role. The ion drag, exerted on the grains by positive ions moving from the discharge center toward the walls, also turned out to be insufficient when the screened Coulomb interaction between ions and grains was based on the linearized Debye length. This force was a factor of five to ten too small. By using the electron Debye length [14] in the expressions for the Coulomb interaction the force became large enough, but this assumption of pure electron screening was unrealistic in the center of the discharge. Since the first observations, the theoretical description of the interaction of the ion flow with the dust particles has shown a significant evolution [15–20]. It was realized that the high floating potential of the dust causes deflection of the ions beyond the Debye length, while ion-neutral collisions enhance the probability for ion capture, reducing the dust charge and enhancing the drag as compared

*Corresponding author: e-mail: W.J.Goedheer@rijnhuizen.nl; Phone: +31 30 6096838, Fax: +31 30 6031204

to the electric force. Also the influence of the ion drift was included [20, 21]. The expression for the ion drag including these improvements yields a force that is large enough to explain the generation of the void.

Based on the understanding of the ion drag force discussed above, we have developed a model for a complex radio-frequency discharge. Other important aspects of the model are the loss of plasma on the dust and the influence of the dust charge on the distribution of the electric potential. This makes the model fully self-consistent. In the next sections, we will first describe the model in more detail and discuss the physics involved. Applications address the mechanism leading to formation of the void and ways to obtain a homogeneous dust distribution. Experiments on board of the International Space Station have shown that it is possible to close the void by reducing the power applied to the discharge [22]. Simulation results of these experiments are presented, as well as results for a discharge containing less particles. This enabled a study of the transition, back and forth, from a homogeneous dust distribution to a fully developed void. Finally, simulations are discussed for a discharge on earth, where gravity is balanced by thermophoresis.

Since experiments are usually performed at low gas pressures, the energy distribution of the electrons no longer depends on the local plasma parameters only. Their mean free path for energy loss becomes comparable to the characteristic gradient lengths or even to the electrode distance. A hydrodynamic description fails to resolve this and a kinetic approach is needed [23]. An often applied technique is the Particle-In-Cell plus Monte Carlo approach [24, 25]. Test electrons and ions, each representing a large amount of real ones (their weight) are followed on their way through the discharge. Their instantaneous spatial distribution enables the calculation of the net space charge and the self-consistent electric field. Collisions with dust grains can be added in the MC model and the dust charge can be accounted for in the Poisson equation. A one-dimensional PIC/MC model will be presented and applied to discharges with an immobile prescribed distribution of grains. Applications of the model include the behaviour of the dust charge with pressure and in modulated discharges.

2 Hydrodynamic modelling

2.1 Description of the plasma

To model complex radio-frequency discharges under microgravity, a standard discharge model must be coupled to a description of the dust grain fluid, accounting for all relevant interactions that lead to the coupling between the plasma and the dust. The description of the plasma is based on the particle balance for electrons and positive ions, with drift-diffusion expressions for the fluxes, $\vec{\Gamma}_j$ [26]:

$$\frac{\partial n_j}{\partial t} + \vec{\nabla} \cdot \vec{\Gamma}_j = S_j, \qquad \vec{\Gamma}_j = n_j \mu_j \vec{E} - D_j \vec{\nabla} n_j. \tag{1}$$

Here, μ_j is the mobility and D_j the diffusion coefficient for species j. The source, S_j, contains plasma recombination on the surface of the dust particles. The electric field, $\vec{E}$, is found from the Poisson equation, that includes the dust particle charge:

$$\Delta V = -\frac{e}{\epsilon_0}\left(n_+ - n_e - Z_d n_d\right), \qquad \vec{E} = -\vec{\nabla} V. \tag{2}$$

Here, Z_d is the dust particle charge number, and n_+, n_e, and n_d are the positive ion, electron, and dust particle densities respectively. Since radio-frequency discharges are usually driven at frequencies above the ion plasma frequency, inertia inhibits an instantaneous adjustment of the ions to changes in the electric field. This can be accounted for by replacing the actual electric field in the expression for the flux by an effective field $\vec{E}_{eff}$. Assuming a dominance of the drift contribution, and neglecting momentum transport, an evolution equation can be derived for this effective electric field [27]:

$$\frac{\partial \vec{E}_{eff}}{\partial t} = \nu_m \Big(\vec{E} - \vec{E}_{eff} \Big), \qquad \nu_m = \frac{e}{\mu_+ m_+}. \tag{3}$$

In this equation ν_m is the momentum loss frequency, and m_+ is the ion mass. The energy balance for the electrons is solved using a similar drift-diffusion approximation for the electron energy density $w = n_e \epsilon$, with ϵ

the average electron energy. The power input is Ohmic heating. Losses, S_w, come from inelastic collisions with the background gas (computed with a two-term Boltzmann solver) and capture of electrons by the dust.

$$\frac{\partial w}{\partial t} + \vec{\nabla} \cdot \vec{\Gamma}_w = -e\vec{\Gamma}_w \cdot \vec{E} + S_w, \qquad \vec{\Gamma}_w = \frac{5}{3}\Big(\mu_e w\vec{E} - D_e\vec{\nabla}w\Big). \tag{4}$$

The ions are assumed to dissipate their power locally in collisions with the gas. Their energy balance is not solved. Only the dissipated power is computed, being a contribution to the total power balance of the discharge.

2.2 Description of the dust fluid: charging

Dust particles introduced in a plasma collect ions and electrons and charge up to the floating potential with respect to the surrounding plasma. When the surface of the dust particle is at floating potential, the currents of electrons and ions towards the surface of the dust particles are equal. The current of ions and electrons to a spherical dust particle of radius a is obtained from the Orbital Motion Limited theory (OML) [28]. This theory does not include the effect of collisions, the angular momentum is assumed to be conserved. If the collision mean free path becomes comparable to the Debye length, however, the ion current is enhanced by ion-neutral collisions that reduce the ion velocity [16]. The modified currents are given by:

$$I_+ = 4\pi a^2 e n_+ \sqrt{\frac{E_+}{2m_+}}\Big[1 - \frac{eV(a)}{E_+} + 0.1\left(\frac{eV(a)}{E_+}\right)^2 \frac{\lambda_D}{l_{mfp}}\Big], \tag{5}$$

$$I_e = -\,4\pi a^2 e n_e \sqrt{\frac{kT_e}{2\pi m_e}} \exp\left(\frac{eV(a)}{kT_e}\right), \tag{6}$$

where E_+ is the energy of the ions consisting of the thermal energy (assuming a Maxwellian distribution) and the kinetic energy resulting from the drift velocity u_+ in the electric field:

$$E_+ = \frac{4kT_{gas}}{\pi} + \frac{1}{2}m_+ u_+^2. \tag{7}$$

In the above equations a is the dust particle radius and T_e the electron temperature. λ_D and l_{mfp} are the linearized Debye length and the mean free path for ion-neutral collisions. Equating $I_+ = -I_e$ gives the equilibrium floating potential, $V_{fl}(a)$ and the dust charge is then given by $eZ_d = 4\pi\epsilon_0 a V_{fl}(a)$.
Collisions with neutrals also affect scattering of ions, this is discussed in the next paragraph, dealing with the forces acting on the dust.

At the floating potential, the electrons and ions arriving at the dust particle will recombine at a rate $n_d I_e/e$. The energy released is used to heat up the particle surface, and is mostly cooled away in collisions with the atoms of the background gas. This heats the gas, adding to the power dissipated by the plasma ions, thus establishing a temperature gradient. The energy flux absorbed by the dust grains, J_{rec}, is given by:

$$J_{rec} = n_d n_e \sqrt{\frac{k_B T_e}{2\pi m_e}} \exp\left(\frac{eV_{fl}}{k_B T_e}\right) E_i, \tag{8}$$

with V_{fl} the floating potential and E_i the ionisation energy of the gas. The power loss, Q_{out}, consists of two contributions. Thermal transfer to the gas,J_{th}, and radiative loss, J_{rad}. For the pressure range in the microgravity experiments, the thermal transfer is governed by the Knudsen theory [29, 30] and given by:

$$J_{th} = \frac{\gamma + 1}{16(\gamma - 1)} \frac{p}{\sqrt{T_g}} \sqrt{\frac{8k_B}{\pi m_g}} \alpha (T_p - T_g). \tag{9}$$

Here $\gamma = c_p/c_v$ is the heat capacity ratio, m_g is the gas atomic mass, p is the gas pressure, T_p is the dust particle surface temperature, T_g is the gas temperature and α is the accommodation coefficient. The radiative cooling term J_{rad} follows directly from the Stefan-Boltzmann law:

$$J_{rad} = \epsilon\sigma\left(T_p^4 - T_w^4\right), \tag{10}$$

in which ϵ is the emissivity, σ is the Stefan-Boltzmann constant and T_w is the reactor wall temperature. For an argon discharge $\gamma = 5/3$ and $\alpha = 0.86$ have been suggested in the literature [31]. The emissivity of the melamine-formaldehyde (MF) particles that are mostly used in the experiments is assumed to be 0.9 [32]. Equations (8) and (9) are coupled to the temperature balance for the gas and solved with an iterative method.

2.3 Description of the dust fluid: forces

Regarding the forces, the electrostatic force and gravity follow directly from the charge, the time averaged electric field, $\vec{E}_{av}$ and mass m_d of the dust grains:

$$\vec{F}_{el} = eZ_d\vec{E}_{av}, \qquad \vec{F}_g = m_d\vec{g} = \frac{4\pi}{3}a^3\rho_d\vec{g}. \tag{11}$$

If the background gas is assumed to be at rest, the neutral drag acting on the dust particles moving through the background gas is proportional to the dust drift velocity, $\vec{v}_d$. The temperature gradient in the background gas causes the thermophoretic force.

$$\vec{F}_n = -\frac{4}{3}\pi a^2\rho_{gas}v_{th}\vec{v}_d, \qquad \vec{F}_{th} = -\frac{32}{15}\frac{a^2}{v_{th}}\kappa_T\vec{\nabla}T_{gas}. \tag{12}$$

Here ρ_{gas} is the mass density, and v_{th} the average thermal velocity of the background gas. κ_T is the translation part of the thermal conductivity (0.0177 $\mathrm{WK^{-1}m^{-1}}$ for Ar at 300 K).

The spatial distribution of the gas temperature is obtained from the heat balance, with a prescribed temperature at all parts of the reactor wall and electrodes, and an axis of symmetry at r=0.

$$\vec{\nabla}\cdot\left(-\kappa_T\vec{\nabla}T_{gas}\right) = 4\pi a^2 n_d J_{th} + e\vec{\Gamma}_i\cdot\vec{E} \tag{13}$$

The ion drag consists of two parts: the transfer of momentum by ions *collected* and the transfer of momentum by ions *deflected* by the dust particle. The force is given by:

$$\mathbf{F}_{id} = m_+\int \mathbf{v}vf_+(v)\left[\sigma_c(v)+\sigma_s(v)\right]d\mathbf{v}. \tag{14}$$

$\mathbf{v}$ is the total ion velocity and $f_+(v)$ is the ion velocity distribution function. The cross section for ion capture $\sigma_c(v)$ is found from OML theory:

$$\sigma_c(v) = \pi a^2\left(1+\frac{\rho_0(v)}{a}\right), \tag{15}$$

with $\rho_0(v) = Z_De^2/2\pi\epsilon_0 m_+v^2$ the Coulomb radius. The cross-section for deflection, or scattering, depends on the specific form of the potential around the dust particle. It is found from:

$$\sigma_s(v) = 4\pi\int_{b_{min}}^{b_{max}}\frac{bdb}{1+(b/\rho_0(v))^2} = 4\pi\rho_0^2(v)\Lambda(v), \tag{16}$$

where b is the impact parameter of the ion approaching the dust particle and $\Lambda(v)$ is called the Coulomb logarithm. The original approach [33] uses:

$$\Lambda(v) = \frac{1}{2}\ln\left[\frac{\rho_0^2(v)+b_{max}^2}{\rho_0^2(v)+b_{min}^2}\right]. \tag{17}$$

b_{min} is the collection cross section given by equation (15). The approach by [34] is to include ions scattered beyond the screening length, by chosing $b_{max} = \lambda_D(v)(1+\rho_0(v)/\lambda_D(v))^{1/2}$. $\lambda_D(v)$ is the linearized Debye length, based on the standard electron Debye length, $\lambda_D(n_e, T_e)$ and the ion Debye length, $\lambda_D(n_+, E_+)$ derived from the total ion energy, $m_+v^2/2 = E_+$. The Coulomb logarithm now becomes:

$$\Lambda(v) = \ln\left[\frac{\rho_0(v)+\lambda_D(v)}{\rho_0(v)+a}\right], \tag{18}$$

which results in an increased ion drag force when the linearized Debye length is used. The above form of the Coulomb integral is valid for $\beta(v) = \rho_0(v)/\lambda_D(v) \leq 5$ which is usually the case inside a dust cloud and near the edge of a void. Inside a void $\beta(v) \gg 1$. In this case a better form of the scattering cross section is given by $\sigma_s(v) = 4\pi\rho_0^2(v) \times 2/(1+\beta^{1.65}(v))$ [35]. We did not use this form of the scattering cross-section here.

The above equation is not correct for larger ion flow speed (with thermal Mach number $M_T = u_+/v_T >> 0.55u_b/v_T$, with $u_b = (kT_e/m_+)^{1/2}$ the Bohm speed. [36]). Hutchinson used a PIC approach [36] to calculate the ion drag for higher ion flow speed and he found that good agreement can be found when in the calculation of the Coulomb logarithm, the velocity as given in the total ion energy:

$$v^2 = \frac{8kT_{gas}}{\pi m_+} + u_+^2 \tag{19}$$

is replaced by:

$$v^2 = \frac{8kT_{gas}}{\pi m_+} + u_+^2 \times \left[1 + \left(\frac{u_+}{u_b}/\left(0.5 + 0.05 \quad ln(\tilde{m}_+/Z_+) + (T_i/T_e)^{1/2}\right)\right)^3\right], \tag{20}$$

where $\tilde{m}_+$ is the ion mass in amu ($\tilde{m}_+/Z_+ = 40$ for argon ions).

When ions collide with background neutrals and the mean free path becomes comparable to or smaller than the screening length, more ions can be effectively deflected by the dust particles, since they lose angular momentum in these collisions. This is not accounted for in the OML model, where angular momentum is conserved. In [18, 19] a theoretical description was constructed for the calculation of the ion drag force, including these collisions by adding a "collisional function", $\mathcal{K}$, to the Coulomb integral. The complete expression of the ion drag force in the model is given by:

$$\begin{aligned} \vec{F}_{id} &= \vec{F}_{id}^{c} + \vec{F}_{id}^{o}, \\ &= n_+ m_+ v\vec{u}_+ \times \left(\sigma_c(v) + \pi\rho_0^2(v)\left[\Lambda(v) + \mathcal{K}\Big(\frac{\lambda_D(v)}{l_{mfp}}\Big)\right]\right), \end{aligned} \tag{21}$$

with

$$\mathcal{K}(x) = x\arctan(x) + \left(\sqrt{\frac{\pi}{2}} - 1\right)\frac{x^2}{1+x^2} - \sqrt{\frac{\pi}{2}}\ln(1+x^2). \tag{22}$$

2.4 Description of the dust fluid: drift-diffusion flux

When the density of the grains becomes so large that screening is no longer complete, the potential energy at the average particle distance exceeds the thermal energy of the grains. As a result of that the dust fluid becomes incompressible, and the internal pressure has to be added to the forces. The pressure of a crystalline dust grain distribution, taken from [37], can be written as:

$$P_{cr} = \frac{1+\beta\kappa}{3\beta} N_{nn}\Gamma P_d \exp(-\beta\kappa), \qquad \Gamma = \frac{e^2 Z_d^2}{4\pi\epsilon_0 \Delta k_B T_d}, \tag{23}$$

where Γ is the so-called coupling parameter, $\Delta = n_d^{-\frac{1}{3}}$ is the mean interparticle distance, $\kappa = \Delta/\lambda_D$, with λ_D the linearized Debye length, and $P_d = n_d k_B T_d$ is the non-crystalline pressure. N_{nn}, the number of nearest neighbours, and β are lattice parameters (N_{nn}=8 and β=1.09 for bcc and N_{nn}=12 and β=1.12 for both fcc and hcp lattices).

P_{df}, the dust fluid pressure used, is an interpolation between the non-crystalline and the crystalline pressure, $P_{df} = xP_{cr} + (1-x)P_d$, where the interpolation factor x depends on the coupling factor. If $\Gamma < 1$ then x=0 and if $\Gamma > \Gamma_{crit}$ x=1. In between we use a linear interpolation [37]:

$$x = \frac{\Gamma - 1}{\Gamma_{crit} - 1}, \qquad \Gamma_{crit} = 106\frac{\exp(\kappa)}{1 + \kappa + 0.5\kappa^2} \tag{24}$$

This critical coupling factor is an approximation to the crystal-liquid transition curve, obtained from molecular dynamics simulations for a Yukawa system [38].

Assuming that the damping neutral drag force balances all the other forces, we can now derive a drift-diffusion expression for the dust particle flux:

$$\vec{\Gamma}_d = n_d(m_d\nu_{md})^{-1}\left[\vec{F}_{el} + \vec{F}_{th} + \vec{F}_{id}\right] - D_d\vec{\nabla}n_d. \tag{25}$$

where the diffusion coefficient D_d is given by

$$D_d = \frac{1}{m_d\nu_{md}}\frac{dP_{df}}{dn_d}. \tag{26}$$

and the momentum loss frequency, ν_{md} is defined by:

$$m_d\nu_{md} = \frac{4}{3}\pi a^2\rho_{gas}v_{th}. \tag{27}$$

The forces in this drift-diffusion expression are all averaged over one radio-frequency period. With this choice we also neglect the total time derivative in the momentum balance, restricting ourselves to slowly varying or stationary dust grain distributions. Modelling of waves and instabilities is thus excluded.

3 Sustainment and closure of the void

In this section, we will present simulations of dust grain distributions under micro-gravity conditions, concentrating on the behaviour of the void. We have simulated discharges in the PKE-Nefedov reactor [13]. This reactor is up-down symmetric, with an electrode separation of 3 cm. The total radius is 5 cm, the radii of the electrodes and the electrode shield are 2.1 and 2.4 cm, respectively. The discharge is driven at 13.56 MHz, in push-pull mode.

The first item addressed is the sustainment of the void. The ion drag force is generated by the ions created inside the void, so the ionization rate must have its maximum there. Figures 1a and 1b show the dust density and the electron density, figures 2a and 2b the ionization rate and the Ohmic heating of the electrons in a discharge containing 500,000 particles of 6.8 μm radius, driven at a peak-to-peak voltage of 100V, at a pressure of 27 Pa. The electron heating takes place inside the dust cloud, where the electron density is depleted and the electric field is high. However, the heat is transported via the drift of electrons against the electric field, toward the center, inside the void, where it is used for ionization. This is illustrated in figure 3, where the electron energy flux along the symmetry axis is shown. Inside the dust cloud the flux builds up, while in the void it decreases due to ionization and excitation losses. This mechanism also exists in a dust free discharge. A detailed discussion of this mechanism can be found in [39].

The existence of a void is accompanied by a significantly enhanced density inside the void, as compared to a dust free discharge. This is illustrated in figures 4a and 4b, for a discharge with 500,000 particles of 3.4 μm, at 32V and 27 Pa. Figure 4a shows the dust density, figure 4b the ion density, electron density, dust charge, and net space charge for the discharge with dust, as well as the ion density without dust.

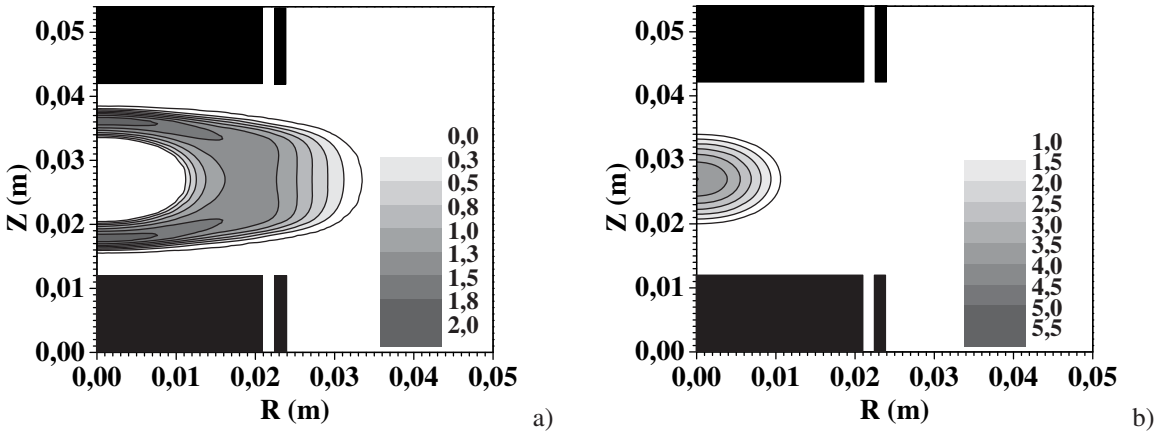

Fig. 1 Dust density in 10^{10} m^{-3} (a) and electron density in 10^{15} m^{-3} (b), for a discharge with 500,000 particles of 6.8 μm radius, driven at 100 V, at a pressure of 27 Pa.

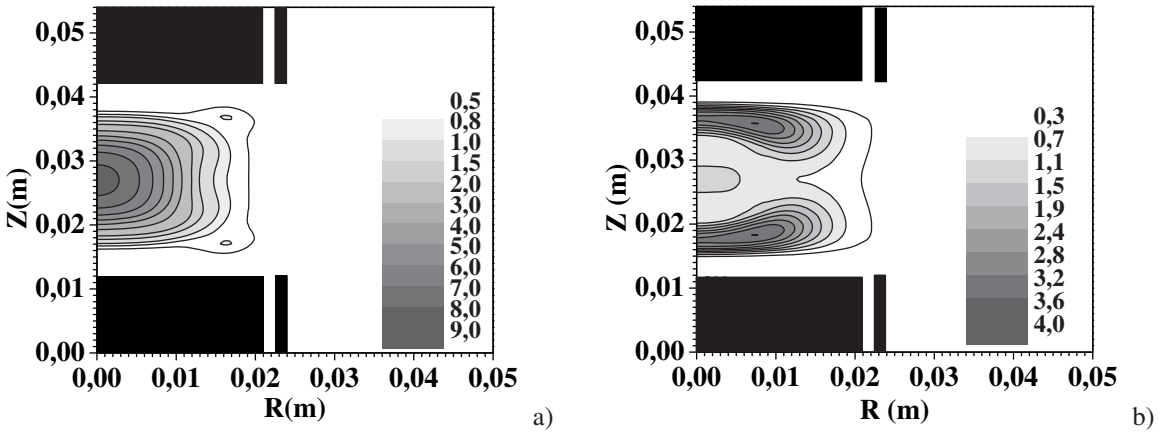

Fig. 2 Ionization rate in 10^{20} m^{3}s^{-1} (a) and Ohmic electron heating in kWm^{-3} (b) for the discharge of figure 1.

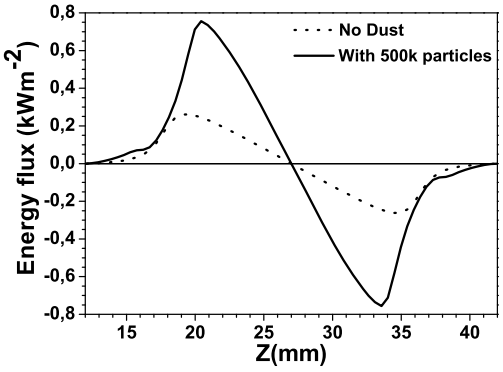

Fig. 3 The electron energy flux along the symmetry axis for the discharge of figure 1.

One way to close the void, is by reducing the power supplied to the discharge. In the experiment discussed in [22], the RF voltage was gradually decreased, resulting in a decrease in the size of the void. The experiment was analyzed with a model for a dust free discharge, studying the behavior of the so-called virtual void, that is

the region inaccessible to a dust particle in a situation where the dust density is too low to change the plasma parameters. From the calculated ion drag and electric force along the symmetry axis, one could derive that the void closes when the central ion density is below a critical value. This analysis, however did not include features due to the strong coupling between the plasma and the dust, such as the enhanced density inside the void. To study the consequences of this coupling, we have simulated the experiment with our self-consistent model, considering the contour with 10^9 particles per cubic meter as the void edge. This rather arbitrary value is low compared to the maximum dust density of approximately 2x10^{10} m^{-3}, and taking an even lower value has no significant influence. Figure 5a summarizes the results obtained for the behaviour of the size of the void, figure 5b shows the behaviour of the central ion and electron density.

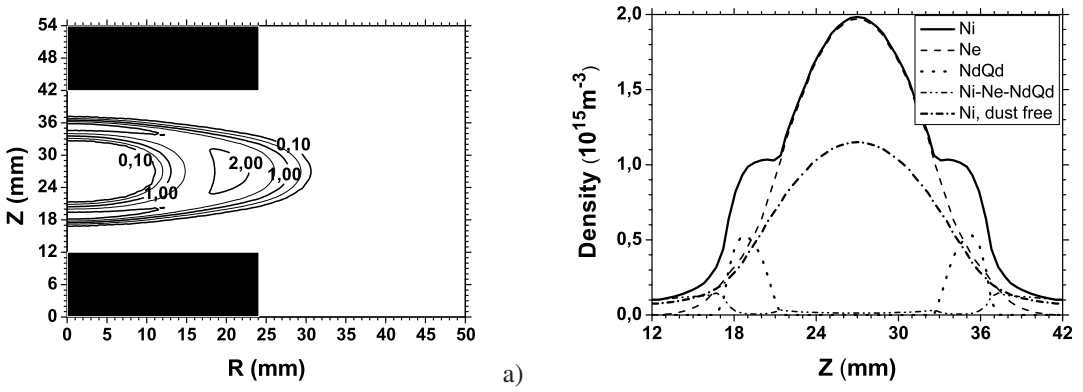

Fig. 4 Dust density in 10^{10} m^{-3} (a) and density profiles along the symmetry axis m^{-3} (b) for a discharge with 500,000 particles of 3.4 μm at 32 V and 27 Pa. Plotted are the ion density (solid line), the electron density (dashed), the charge on the dust, expressed in number of electrons (dotted) and the net charge density (dash-dot-dot). For comparison also the ion density in a dust free discharge is given (dash-dot)

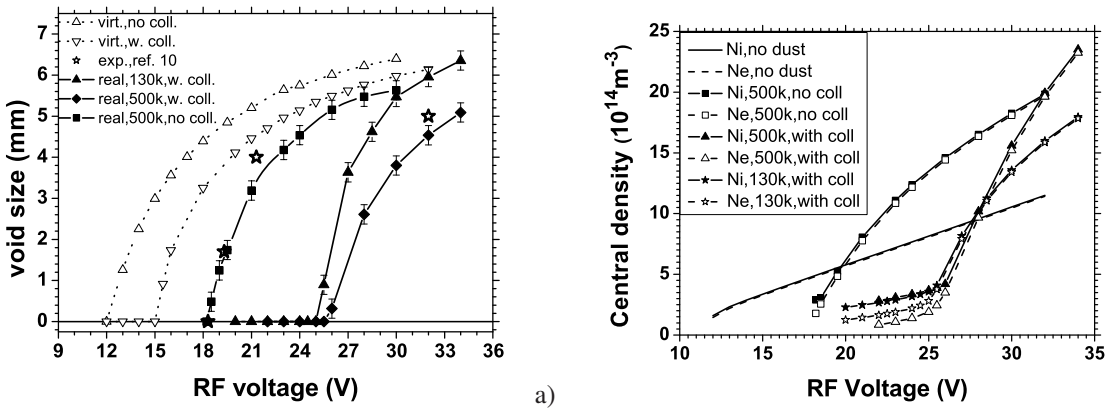

Fig. 5 Behaviour of the real and so-called virtual void size for various discharges as a function of the applied voltage (a) and the corresponding central ion and electron density in 10^{14} m^{-3} (b).

First there is the virtual void size for the case with and without the influence of collisions on the charge, that is, with or without the mean free path dependent part in equation (5). The influence of collisions in the scattering part of equation (21) is always included. The void size is obtained from the point where the net force is zero along the discharge axis, thus measuring the void height. The reduced charge shifts the curve to higher voltages. Next, the full curves show the real void size, obtained from the dust contour, for a simulation with 500,000 particles, again with and without collisions. The case without collisions matches the experimental data given in [22] very well, ending in a closed void at 18.2 V, against 18.3 V in the experiment. With the effect of collisions the curve shifts again, actually away from the experimental data. An analysis of the effect of the collisions is complicated

by the associated changes, both in the forces and in the plasma density. At a large amount of dust grains, the loss of plasma due to recombination can become so high that the discharge can no longer be sustained. Note that electrons are needed to provide the ions lost on the dust, a pure dust-ion plasma cannot exist in steady state. As in the experiment, the plasma is operated near to this limit, and just below the point where the void closes, the plasma cannot exist in steady state. We have also done simulations with less particles (130,000), to be able to study the complete transition from a closed Yukawa system to a fully developed void. This case is also presented in figures 5a and 5b.

The behaviour of the central density shows that in the presence of dust, in case the void exists, the density exceeds that of a dust free discharge, a situation also shown in figure 4b. At closure, the density decays below the critical density which is lower than the density in a dust free discharge at the same voltage. The dust free discharge at this voltage thus still shows a virtual void. Combining figures 5a and 5b, for the cases with the effect of collisions on the charge, shows that the void in all cases closes at the same ion density, in agreement with theory (figure 6a). When a dust free discharge is loaded with a small amount of grains, the virtual void appears. Enhancing the number of grains will make the void smaller (by reducing the central ion density), until the void is closed. The amount of grains needed to reduce the ion density to the critical value where the void is fully closed will depend on the RF voltage. Figure 6b shows the minimum amount of dust at which the void closes as a function of the RF voltage. At closure, when the central dust density is 10^9 grains per cubic meter, the density is again approximately the same in all cases, namely $2.5{\cdot}10^{14}\mathrm{m}^{-3}$.

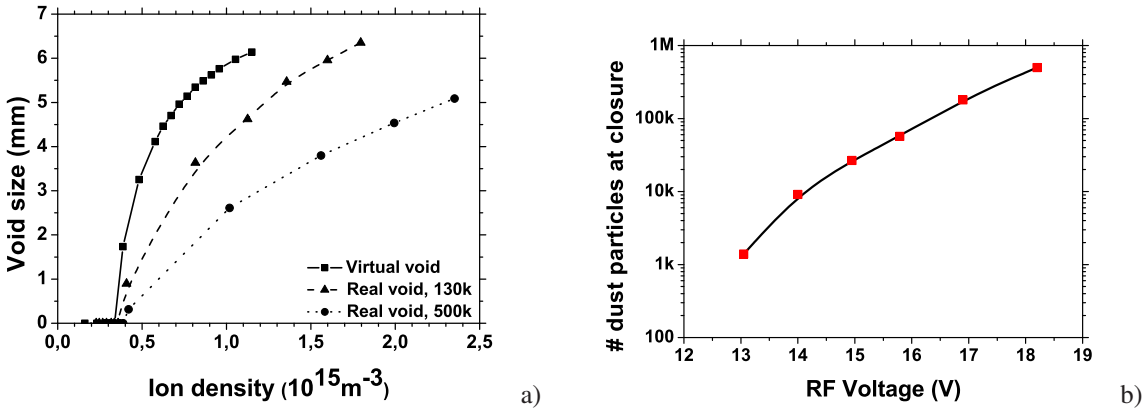

Fig. 6 Void size versus central ion density, showing the same conditions for closure (a) and the minimum amount of dust particles (of 3.4 μm at which the void closes for a given rf voltage (b).

The dust distributions with 130,000 particles could also be reproduced by a procedure in which we started with a low power, where the virtual void does not exist, so the dust immediately accumulates in the center. Gradually enhancing both the power and the amount of dust then yielded the same profiles as obtained by starting at a high power, injecting all the dust, and reducing the power to close the void.

Figure 7a shows the dust density distribution for 130k particles, at 20V, with the effect of collisions on the charge included. The distribution is very homogeneous. This is caused by the strong reduction of the forces. As shown in figure 7b, the forces are considerably smaller than in the dust free case. The electric field is strongly reduced by the electronegative character of the discharge, and the ion drag force is small because of the low ion density. In case of a fully developed void the opposite happens, the enhanced ion density results in an ion drag that exceeds the one in the dust free discharge [40].

The simulations discussed above can also assist in understanding the behaviour of small dust grains penetrating a cloud of larger grains. For smaller grains the ion drag force is less effective, so when they are injected they tend to move through the cloud of larger grains and settle inside the void, thus creating a smaller void. When the difference in size is large enough, a clear separation is observed in the final distribution. The force acting on the small particles, however, is strongly affected by the presence of the large grains. Figure 8a shows the distribution of dust particles with a radius of 9 μm in a discharge driven at 32 V, at 27 Pa. When particles of 3.4 μm radius are released in the midplane, they form lanes [3], drifting toward the center. Figure 8b shows the radial force acting

on the large and small grains. For the large grains there is a zone where the net force is practically zero, the small grains feel an inward force everywhere, up to a point inside the void.

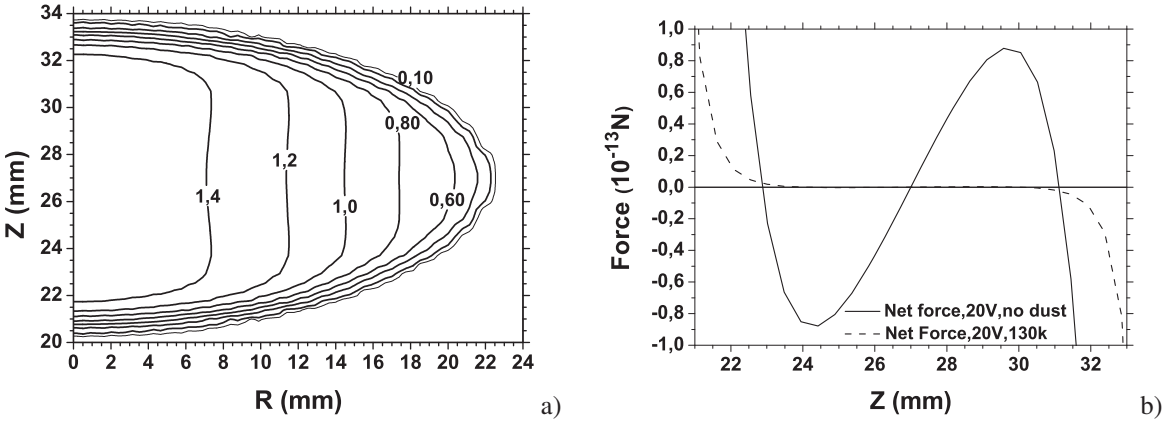

Fig. 7 Dust density distribution (in $10^{10}\mathrm{m}^{-2}$) at 20V, with 130k particles, showing the homogeneity of the resulting Yukawa ball (a) and the net axial force along the axis of the discharge (b). For comparison also the net force in a dust free discharge is shown

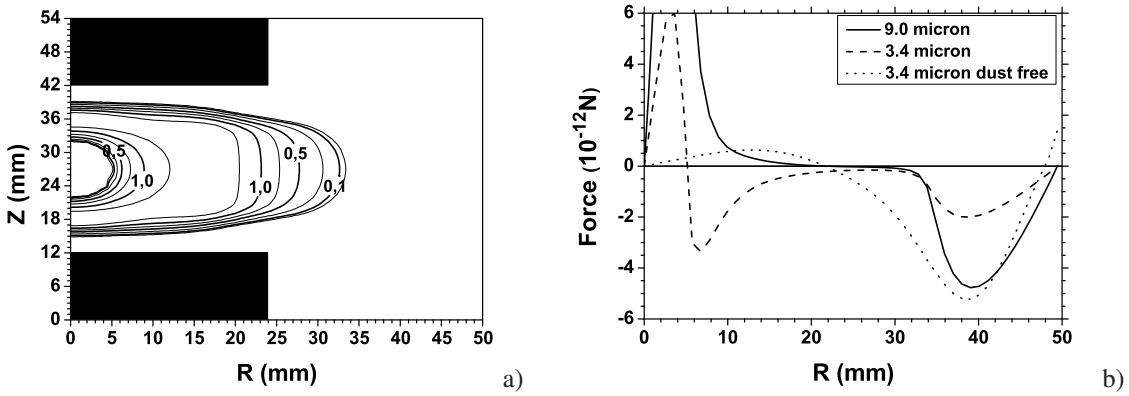

Fig. 8 Dust density distribution (in $10^{10}\mathrm{m}^{-3}$) for 9μm radius grains in a discharge operated at 32V, with 500k particles (a), and the radial net force in the plane of symmetry, acting on the 9μm particles and on 3.4 μm particles released from the wall (b).

On earth, gravity can be balanced by means of the thermophoretic force, for one particle size [9, 10]. The 3.4 μm particles in this study require a temperature gradient of 2.23 K/mm. This can be established by cooling of the upper electrode, for instance. Figure 9a shows the dust density distribution for a total of 125,000 particles when the upper electrode is at 233K, while all parts of the wall are kept at 300K. This gives a thermophoretic force that compensates gravity in the axial direction, but at the same time confines the dust cloud radially, see figure 9b. The main disturbing phenomenon in experiments is the generation of Rayleigh-Benard vortices. The temperature distribution easily becomes unstable, governed by the Boussinesq Reynolds number [41]:

$$R^B = \frac{g\alpha\|\Delta T\|d^3}{k_c\nu}, \tag{28}$$

with g the gravitational acceleration, α the coefficient for thermal expansion, κ_c the thermometric conductivity, ν the kinematic viscosity, and ΔT the temperature difference between horizontal plates at a distance d. Taking the values for Argon at 300 K given in [42], for a temperature difference of 100K at a plate distance of 3 cm we arrive at a value $R^B \approx$223, less that the reported critical value of $\approx$1700 [41]. In experiments, however, also

radial temperature gradients exist, making the temperature distribution unstable at a lower temperature difference. This will limit the maximum particle size for which a stable configuration can be found.

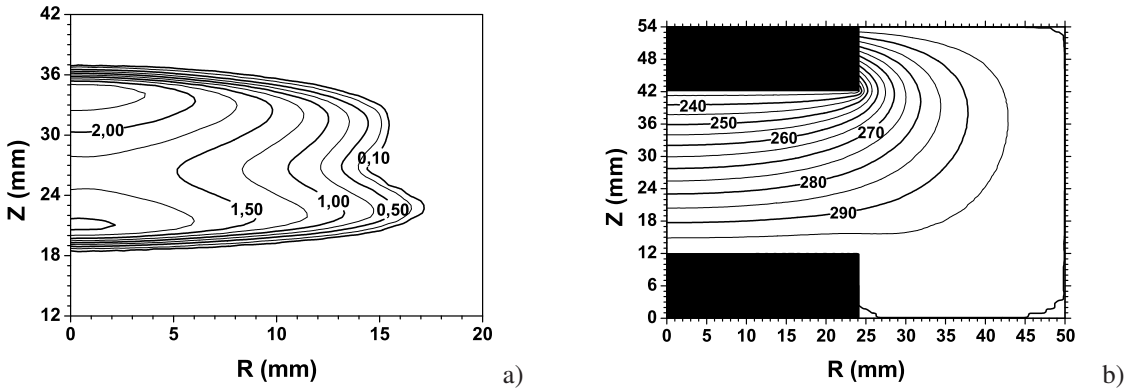

Fig. 9 Dust density distribution (in $10^{10}\mathrm{m}^{-2}$) at 20V, with 125k particles (a), when gravity is balanced by the thermophoretic force produced by the temperature profile generated by cooling the upper electrode (b).

4 Particle-In-Cell plus Monte Carlo modelling

4.1 Including collisions with dust grains

Complex plasma experiments are usually performed in low-pressure discharges, where the mean free path for energy loss of the electrons can easily exceed characteristic gradient lengths. This holds especially for the scale length of the electric field in the sheath. Next to that is the characteristic time for electron energy loss, to be compared with the frequency of the applied RF voltage. Since the charge of a dust particle is governed by the high-energy tail of the electron energy distribution function, typically beyond a few times kT, kinetic effects can become very important.

An appropriate way to model these effects is the Particle-In-Cell plus Monte Carlo approach. This method is based on following a limited amount of electrons and ions on their way through the discharge. Each particle represents a (large) number of real electrons or ions, enabling the calculation of the net space charge, and from that the self-consistent electric field. For a detailed discussion of the method, applied to low-temperature plasmas, we refer to [24, 25]. Here we concentrate on adding collisions with dust grains.

Collisions with the background gas are usually easily implemented in the Monte Carlo part of the simulation. The gas density is constant, rendering the collision probabilities independent of the position in the discharge. This is different for collisions with dust grains. The dust density has a non-uniform distribution with a zero density in the void and in the sheaths, and also the dust charge may vary through the dust fluid or crystal. This implies we have to define the collision probabilities on a computational grid, where the dust density and dust charge are both defined.

The cross sections for capture and scattering of electrons and ions by a dust grain of radius a, with a charge Q, can be approximated by the truncated Coulomb cross section, assuming no screening up to the linearized Debye length and full screening beyond that distance. With this assumption we obtain for capture:

$$\sigma_{capt} = \min\left(\pi a^2\big(1 \pm \frac{Q}{4\pi\epsilon_0 w a}\big), \pi L_{nn}^2\right), \tag{29}$$

where w is the kinetic energy and the cross section is cut off at a distance $L_{nn} = n_d^{-\frac{1}{3}}$, the average distance between the dust grains. The $+$ sign applies for electrons, the $-$ sign for ions in case of a negative dust charge Q. The scattering cross section is:

$$\sigma_{scatt} = \min\left(\pi\lambda_D^2, \pi L_{nn}^2\right) - \sigma_{capt} \tag{30}$$

The local linearized Debye length, λ_D is obtained from the time-averaged energies and densities as:

$$\lambda_D^{-2} = \lambda_{De}^{-2} + \lambda_{Di}^{-2}, \lambda_{De,i}^2 = \frac{2\epsilon_0 < w_{e,i} >}{3e^2 < n_{e,i} >} \tag{31}$$

The scattering angle, ξ is given by

$$\tan(\frac{\xi}{2}) = \frac{b_0}{b}, b_0 = \frac{Q}{8\pi\epsilon_0 w} \tag{32}$$

The model presented here is one-dimensional. Thus in a grid cell of height dz and an area equal to the electrode, πR_{el}^2, there are $N_d dz \pi R_{el}^2$ dust particles. If an electron or ion is captured within the cell, its charge, multiplied by the number of real particles it represents, is added to the dust charge in the cell. Thus, we keep track of the total amount of charge in the cell and the charge of a single dust grain, needed for the cross section is obtained by dividing this total charge by the amount of dust grains in the cell. Thus, with a prescribed grain density, only the charge varies in space and time.

The grid where the dust charge is stored coincides with the grid used for the calculation of the potential distribution in the discharge, obtained by solving the Poisson equation:

$$\frac{d^2V}{dz^2} = -\frac{1}{\epsilon_0}\left(en_i(z) - en_e(z) + Q(z)n_d(z)\right) \tag{33}$$

4.2 Results

We used our PIC/MC model in the past for various studies, including decay of the charge when the discharge is switched off, manipulation of the charge with a source of UV photons, and changes in the discharge current waveform induced by changes in the resistivity [43,44]. Here we present results of a study of the effect of the gas pressure and of power modulated discharges. The influence of the gas pressure is studied for two cases, one with large dust grains, of 6.8 μm radius and one with small grains, having a radius of 0.34 μm. The electrode spacing, L, is 3 cm and a fixed density distribution is prescribed for the dust. The large grain distribution is assumed to have a central void and the density is $2.5{\cdot}10^9\mathrm{m}^{-3}$ for $L/4 < z < 7L/16$ and for $9L/16 < z < 3L/4$, elsewhere it is zero. The small grains have a density of $10^{12}\mathrm{m}^{-3}$ for $5L/16 < z < 11L/16$ and elsewhere zero. With this choice of densities, the grain surface area collecting electrons and ions is the same in both cases. Figure 10 shows the charge (in number of electrons) on a dust grain for both cases, figure 11a and 11b the average electron energy and the ratio between the ion and electron density. Data are given for a point at the center of the dust cloud, so at $x = 11L/32$ for the large grains and at $x = L/2$ for the small grains.

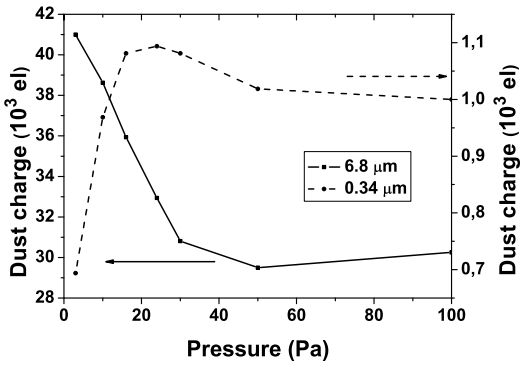

Fig. 10 The charge on the dust grains versus the gas pressure for large grains (6.8 μm) with a void and small grains (0.34 μm) without a void in the density distribution.

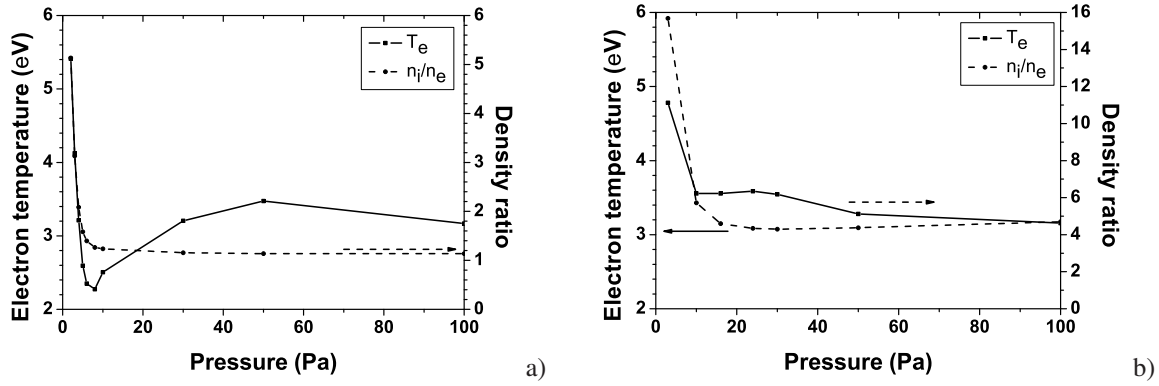

Fig. 11 Behaviour of the average electron energy and the ratio between the ion and electron density for the cases with large (a), and small dust grains (b).

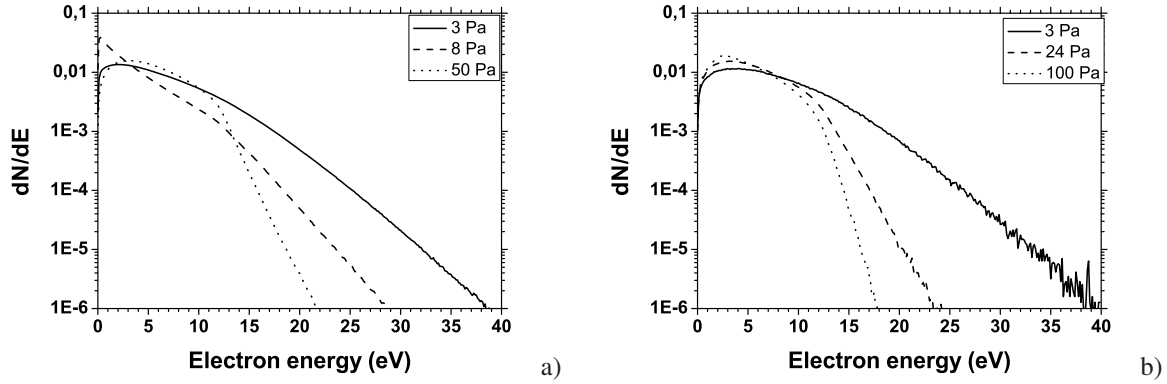

Fig. 12 Normalized electron energy distribution functions at the center of the grain density distribution for large (a) and small (b) grains, showing the variation with pressure.

The dust charge for the large grains rises sharply when the pressure is decreased. This can be attributed to the increase in average electron energy. The electrons show the transition from a local to a non-local behaviour. The effect of the increased electron energy is partly compensated by the growth of the ratio of the ion and electron density, leading to a relatively larger ion current toward the dust surface. At low pressures the electron density drops and the so-called Havnes parameter, $P = Z_d n_d/n_e$ increases. The behaviour of the electron energy distribution function (EEDF), shown in figure 12a, reflects the non-local behaviour. At low pressures the EEDF has a strongly populated high energy tail. For the small grains the same holds, but now the density ratio increases even more, overcompensating the electron heating. This is related to our choice of the amount of dust (proportional to a^{-2}) and the fact that the charge roughly goes as $\propto a$. The EEDF for the small grains is shown in figure 12b.

A PIC/MC simulation also allows for a study of charging dynamics. We have simulated the effect of a modulation of the discharge power, alternating the applied voltage between 40 V and 120 V for a discharge operated at 13.56 MHz, at a pressure of 10 Pa, loaded with particles of 3.4 μm radius at a density of $10^{10}\mathrm{m}^{-3}$, with a void as before for the 6.8 μm particles. At switch-off, the electrons rapidly cool down and the dust charge (in number of electrons) decreases due to capture of positive ions. The electron density decreases on the timescale of ambipolar diffusion, typically 10 μs, or 100 RF cycles. When the discharge is not switched on again, a small charge remains, due to the plasma loss at the walls [45] When the power is raised again, the remaining electrons become hot and start to recharge the grains. We investigated the behaviour of the charge for modulation frequencies of 33.9 KHz (period 400 RF cycles), 13.56 kHz (1000 cycles) and 6.78 kHz (2000 cycles). The modulation period is thus first in the range of the ambipolar decay time and is increased by a factor of 2.5 and 5. The results are presented in figures 13a through 13c, as the sum over all grid points of the electrons on the dust. The longer the period with

low power, the more the electron density drops, enhancing the overshoot phenomenon. However, there is a different mechanism active, namely the behaviour of the electron energy and density with power. At low powers the electron density is lower and the electron energy is higher than at high power. Due to this the modulation of the grain charge is partly reversed, especially at low modulation frequencies (figure 13c). The charge first drops, due to the cooling, but when the discharge approaches the periodic steady state corresponding to the low power, the dust charge rises again. Then, there is the overshoot at switching to high power, but the discharge now wants to settle at a grain charge lower than that in the low power discharge. When the modulation period is made shorter, the periodic steady states are beyond reach, and the charge more or less follows the applied power (figure 13a).

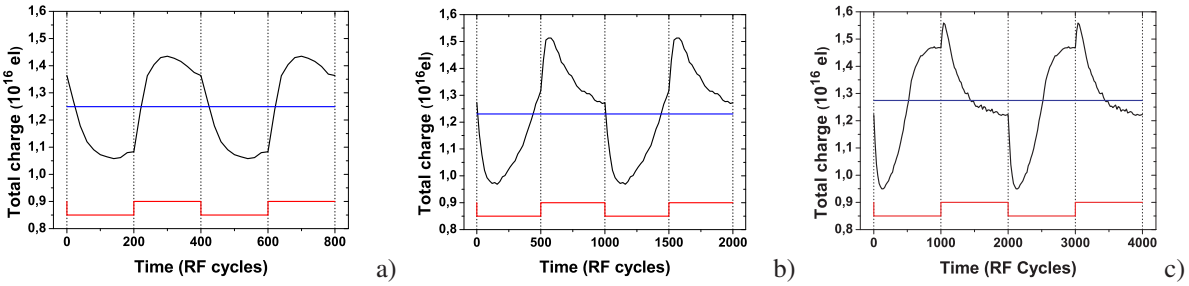

Fig. 13 Variation of the dust charge in a modulated discharge with a modulation period corresponding to 400 (a), 1000 (b), and 2000 (c) RF cycles. The pressure is 10 Pa and the RF frequency is 13.56 MHz.

Experiments with modulated discharges in acetylene show a significant increase of the electron density at switch-off [46]. The mechanism behind this is not yet clearly identified. Possibly field emission plays a role, promoted by a low work function for carbonaceous dust. The Fowler-Nordheim expression [47] predicts the emitted current as

$$I_{FN} = 4\pi a^2 \frac{e^2 E^2}{8\pi h\phi t^2(y)} \exp\left(-\frac{8\pi\sqrt{2m_e}\phi^{3/2}}{3heE} v(y)\right), \tag{34}$$

with ϕ the work function, E the electric field, $t(y) \approx 1 + 0.1107y^{1.33}$, $v(y) = 1 - y^{1.69}$. The argument y is

$$y = \frac{1}{\phi}\sqrt{\frac{e^3 E}{4\pi\epsilon_0}} \tag{35}$$

The exponential function in this expression usually renders the emission unimportant. For small particles, with a size up to ≈10 nm, the electric field at the grain surface can exceed 10^9 V/m, and field emission becomes relevant (depending on the work function) The emission may be promoted by an enhanced field resulting from a reduction of the Debye length at switch-off.

5 Conclusions and a view on future modelling

The theoretical insight in the ion drag force exerted on a dust particle has reached a level where realistic simulations of complex plasmas are possible. The simulations presented in this paper show good agreement with experiments on closure of the dust free void inside a dust cloud under microgravity conditions. Using the fact that at a low ion density the inward electric force exceeds the outward ion drag force, the formation of large homogeneous dust distributions, Yukawa balls, exceeding 100,000 particles, is possible. Balancing gravity by the thermophoretic makes this regime accessible on earth as well.

Still missing are full non-linear simulations of waves and instabilities. When these phenomena occur, the amplitudes are large and the relatively slow evolution of the dust density and charge will lead to significant changes in the local plasma parameters. This has to be modelled self-consistently. The models discussed in this paper need only relatively small modifications. When the full dust momentum balance is included they should be able to deal with these phenomena, since the full dust-plasma interaction is already implemented.

Another issue that should be addressed in more detail is the interaction between the dust and the plasma when a crystal has been formed. The expressions for momentum transfer and charging start from the assumption that grains are completely shielded. Probably this also resolves one of the characteristics of the dust surrounding a void, namely the enhanced density near the void edge. The hydrodynamic models fail to reproduce that.

For studies of kinetic effects the Particle-In-Cell approach provides excellent possibilities. Non-local effects can easily be captured and dynamics of dust charging and de-charging can be studied over the whole pressure range accessed by experiments. PIC/MC models can also assist in revealing the details of a plasma interacting with a crystalline region, discussed above. For that, the PIC/MC models must be made at least 2d-3v, they must resolve two dimensions, as will be clear from the discussion of the mechanism sustaining the void. The maximum heating of the electrons takes place off axis, inside the dust cloud. At low pressures the heated electrons will move through the whole dust cloud and have their maximum kinetic energy inside the void, where the plasma potential has its maximum.

Acknowledgements This work supported by the European Communities under the Association between EURATOM/FOM, was carried out within the framework of the European Fusion Programme with financial support from NWO. The views and opinions expressed herein do not necessarily reflect those of the European Commission.

References

[1] A. Melzer, S. Nunomura, D. Samsonov, and J. Goree, Phys. Rev. E **62** 4162–4171 (2000).
[2] S. Nunomura, J. Goree, S. Hu, X. Wang, and A. Bhattacharjee, Phys. Rev. E **65** 1–11 (2002).
[3] A.V. Ivlev, V. Steinberg, R. Kompaneets, H. Höfner, I. Sidorenko, and G.E. Morfill, Phys. Rev. Lett. **98** 145003 (2007).
[4] M. Rubin-Zuzic, H.M. Thomas, S.K. Zhdanov, and G.E. Morfill, New J. Phys. **9** 39 (2007).
[5] S.A. Khrapak, G.E. Morfill, A.V. Ivlev, H.M. Thomas, D.A. Beysens, B. Zappoli, V.E. Fortov, A.M. Lipaev, and V.I. Molotkov, Phys. Rev. Lett. **96** 015001 (2006).
[6] Y. Ivanov and A. Melzer, Phys. Plasmas **12** 072110 (2005).
[7] R. Ichiki, Y Ivanov, M. Wolter, Y. Kawai, and A. Melzer, Phys. Rev. E **70** 066404 (2004).
[8] G.E. Morfill, U. Konopka, M. Kretschmer, M. Rubin-Zuzic, H.M. Thomas, S.K. Zhdanov, and V. Tsytovich, New J. Phys. **8** 7 (2006).
[9] H. Rothermel, T. Hagl, G.E. Morfill, M.H. Thoma, and H.M. Thomas, Phys. Rev. Lett. **89** 175001 (2002).
[10] M. Schwabe, M. Rubin-Zuzic, S. Zhdanov, H.M. Thomas, and G.E. Morfill, Phys. Rev. Lett. **99** 095002 (2007).
[11] O. Arp, D. Block, M. Klindworth, and A. Piel, Phys. Plasmas **12** 122102 (2005).
[12] G.E. Morfill, H.M. Thomas, U. Konopka, H. Rothermel, M. Zuzic, A. Ivlev, and J. Goree, Phys. Rev. Lett. **83** 1598–1601 (1999).
[13] A.P. Nefedov, G.E. Morfill, V.E. Fortov, H.M. Thomas, H. Rothermel *et al.*, New J. Phys. **5** 33 (2003).
[14] M.R. Akdim and W.J. Goedheer, Phys. Rev. E **65** 015401(R) (2001)
[15] S.A. Khrapak, A.V. Ivlev, G.E. Morfill, and H.M. Thomas, Phys. Rev. E **66** 046414 (2002).
[16] S.A. Khrapak, S.V. Ratynskaia, A.V. Zobnin, A.D. Usachev *et al.*, Phys. Rev. E **72** 016406 (2005).
[17] M. Lampe, R.Goswami, Z. Sternovsky, S. Robertson *et al*, Phys. Plasmas **10** 1500–1513 (2003).
[18] A.V. Ivlev, S.A. Khrapak, S.K. Zhdanov, G.E. Morfill, and G. Joyce Phys. Rev. Lett. **92** 205007 (2004).
[19] A.V. Ivlev, S.K. Zhdanov, S.A. Khrapak, and G.E. Morfill, Phys. Rev. E **71** 016405 (2005).
[20] I.H. Hutchinson, Plasma Phys. Contr. Fusion **48** 185–202 (2006)
[21] M. Lampe, G. Joyce, and G. Ganguli, IEEE Trans. Plasma Sci. **33** 57–69 (2005).
[22] A.M. Lipaev, S.A. Khrapak, V.I. Molotkov, G.E. Morfill *et al.*, Phys. Rev. Lett. **98** 265006 (2007).
[23] L.D. Tsendin, Plasma Sources Sci. Technol. **12** S51-S64 (2003)
[24] C.K. Birdsall, IEEE Trans. Plasma Sci. **19** 65–85 (1991).
[25] K. Matyash, R. Schneider, F. Taccogna, A. Hatayama *et al.*, Contrib. Plasma Phys. **47** 595-634 (2007).
[26] V. Land and W.J. Goedheer, New J. Phys. **8** 8 (2006)
[27] A.D. Richards, B.E. Thompson, and H.H. Sawin, Appl. Phys. Lett. **50** 492–494 (1987).
[28] J.E. Allen, Phys. Scripta **45** 497–503 (1992).
[29] M. Knudsen, Ann.Phys. **339** 593–656 (1911).
[30] G.H.M.P. Swinkels, H. Kersten, H. Deutsch, and G.M.W. Kroesen, J. Appl. Phys. **88** 1747–1755 (2000).
[31] R. Piejak *et al.*, Plasma Sources Sci. Technol. **7** 590 (1998).
[32] CRC Handbook of Chemistry and Physics. **75th** ed. (1994).
[33] M.S. Barnes, J.H. Keller, J.C. Forster, J.A. ONeill, and D.K. Coultas, Phys. Rev. Lett. **68** 313 (1992).
[34] S.A. Khrapak, A.V. Ivlev, G.E. Morfill, and H.M. Thomas, Phys. Rev. E **66** 046414 (2002).
[35] S.A. Khrapak, A.V. Ivlev, G.E. Morfill, S.K. Zhdanov, and H.M. Thomas, IEEE Trans. Plasma Sci. **32** 555 (2004).

[36] I.H. Hutchinson, New Vistas in Dusty Plasmas, Proc. 4th Int. Conf. on the Physics of Dusty Plasmas, AIP Conf. Proc. **799** 38 (2005).
[37] G. Gozadinos, A.V. Ivlev, and J,-P.Boeuf, New J. Phys. **5** 32 (2003).
[38] O.S. Vaulina and S.A. Khrapak, JETP **90** 287–289 (2000).
[39] V. Land and W.J. Goedheer, New J. Phys. **9** 246 (2007).
[40] W.J. Goedheer and V. Land, Plasma Phys. Contr. Fusion **12** 124022 (2008).
[41] A.S. Bormann, Continuum Mech. Thermodyn. **13** 9–23 (2001)
[42] E.W. Lemmon and R.T. Jacobsen, Int. J. Thermophysics **25** 21–69 (2004).
[43] V. Land and W.J. Goedheer, IEEE Trans. Plasma Sci. **35** 280–285 (2007).
[44] W.J. Goedheer and Yu.I. Chutov, IEEE Trans. Plasma Sci. **32** 551–554 (2004).
[45] L. Couëdel, A.A. Samarian, M. Mikikian, and L. Boufendi, Phys. Plasmas **15** 063705 (2008).
[46] J. Berndt, E. Kovacevic, V. Selenin, I. Stefanovic, and J. Winter, Plasma Sources Sci. Technol. **15** 18–22 (2006).
[47] N. de Jonge, M. Allioux,M. Doytcheva, M. Kaiser *et al.*, Appl. Phys. Lett. **85** 1607–1609 (2004).

